Neutronics simulations for the design of neutron flux monitors in SPARC

X. Wang ✉ 📧 ; R. Gocht; J. Ball 📧 ; S. Mackie 📧 ; E. Panontin 📧 ; R. A. Tinguely 📧 ; P. Raj 📧 ; I. Holmes 📧 ;
A. A. Saltos; A. Johnson 📧 ; A. Grieve 📧

Check for updates

View
Online

Export
Citation

Neutronics simulations for the design of neutron flux monitors in SPARC

View Online   Export Citation   CrossMark

X. Wang,[1,a)] (ID) R. Gocht,[2] J. Ball,[1] (ID) S. Mackie,[1] (ID) E. Panontin,[1] (ID) R. A. Tinguely,[1] (ID) P. Raj,[2] (ID) I. Holmes,[2] (ID)
A. A. Saltos,[2] A. Johnson,[2] (ID) and A. Grieve[2] (ID)

AFFILIATIONS

[1] Plasma Science and Fusion Center, MIT, Cambridge, Massachusetts 02139, USA
[2] Commonwealth Fusion System, Devens, Massachusetts 01434, USA

Note: This paper is part of the Special Topic on Proceedings of the 25th Topical Conference on High-Temperature Plasma Diagnostics.
[a)]**Author to whom correspondence should be addressed:** wxinyan@mit.edu

ABSTRACT

This paper presents the development and application of high-fidelity neutronic models of the SPARC tokamak for the design of neutron flux monitors (NFM) for application during plasma operations. NFMs measure the neutron flux in the tokamak hall, which is related to fusion power via calibration. We have explored Boron-10 gamma-compensated ionization chambers (ICs) and parallel-plate Uranium-238 fission chambers (FCs). We plan for all NFMs to be located by the wall in the tokamak hall and directly exposed to neutrons streaming through a shielded opening in a midplane port. Our simulations primarily use a constructive solid geometry-based OpenMC model based on the true SPARC geometry. The OpenMC model is benchmarked against a detailed CAD-based MCNP6 model. The B10 ICs are equipped with high-density polyethylene (HDPE) sleeves, borated HDPE housings, and borated aluminum covers to shield out scattered neutrons, optimize detector response levels, and make calibration robust against changes in the tokamak hall. The B10 neutron absorption branching ratio may cause the detectors' responses to be non-linear to neutron flux >200 keV. However, our simulations unveil that, in the SPARC environment and with the proposed housings and sleeves, >99% of the detector responses are induced by <100 keV neutrons. U238's insensitivity to slow neutrons makes this FC a promising candidate for direct fusion neutron measurements. Along with a borated HDPE sleeve, about 60% of the FCs' responses are induced by direct neutrons.

I. INTRODUCTION

Fusion neutrons, as products of DT fusion reactions, carry information about the fusion plasma, including fusion power, ion temperatures, neutron emissivity profiles, etc. Thanks to neutrons' long mean free paths, these parameters can be obtained by measuring neutrons outside the tokamak and away from the harsh plasma environment. Neutron flux monitors (NFM) are one of the neutron diagnostic systems planned for the SPARC tokamak. They measure the local neutron flux in the tokamak hall and convert the measurement to fusion power through calibrations. This paper introduces the OpenMC[1] neutronics modeling work for the design of NFMs for the SPARC[2] tokamak by Commonwealth Fusion Systems (CFS). This paper focuses on two options: B10-coated ionization chambers (IC) and U238 fission chambers (FC). Additional flux-shaping parts

are applied to optimize signal strength, direct/total neutron ratio, robustness of calibrations to changes in the tokamak hall, and flat response. Flat response means DT and DD plasma emitting neutrons at the same rates, despite different energies, should induce the same responses to certain NFMs. B10 ICs and U238 FCs combined are proposed to cover the entire plasma operation range, and more NFMs for the calibration range are under investigation. Calibration neutron sources such as neutron generators and radioactive isotopes are much less powerful than the plasma source during operation, so these calibration-range NFMs must be of a type that has higher sensitivity, such as proportional counters.[3]

The implementation and verification of the OpenMC SPARC model will be covered in Sec. II. Section III will introduce the design and modeling work for the B10 ICs and U238 FCs. The potential

effects of B10's branching ratio in a fast neutron environment will also be discussed. Conclusions and future work on SPARC NFMs will be summarized in Sec. IV.

II. OPENMC SPARC MODEL

A. Model overview

The OpenMC model of SPARC is shown in Figs. 1(a) and 1(b). It features key components, including plasma facing components (PFCs), tokamak vacuum vessel (VV), toroidal field (TF) coils, poloidal field (PF) coils, central solenoid (CS), cryostat, and port shieldings. The PFC has a tungsten layer and a stainless steel (SS, mainly iron and chromium) layer. The 0° midplane port (0MPP) with opened shielding for neutron diagnostics is modeled in more detail for higher fidelity. Other ports are modeled as homogenized blocks with material compositions preserved. The TF coils are modeled as a homogenized Boron Carbide (B4C) + SS case. The cryostat, PF coils, and CS are all modeled as SS. Figure 1(c) is the DT fusion neutron emissivity for SPARC's primary reference discharge (PRD),[3] calculated based on ion density and temperature profiles from the TRANSP code[4,5] and Bosch–Hale reactivities.[6] The boundary of the source touches the PFC because the divertors are not explicitly modeled, but these regions have low emissivity and will not significantly affect the results. OpenMC treats the source as a 50×80 matrix of finite element rings of 14.1 MeV fixed sources thermally broadened by local ion temperature. Within each ring, the volumetric emissivity is uniform.

B. Verification

The OpenMC model is verified with a CAD-based MCNP6[7] model from CFS. Neutron spectra in a shell just outside the tokamak, i.e., in the tokamak hall, are compared. Both the models were
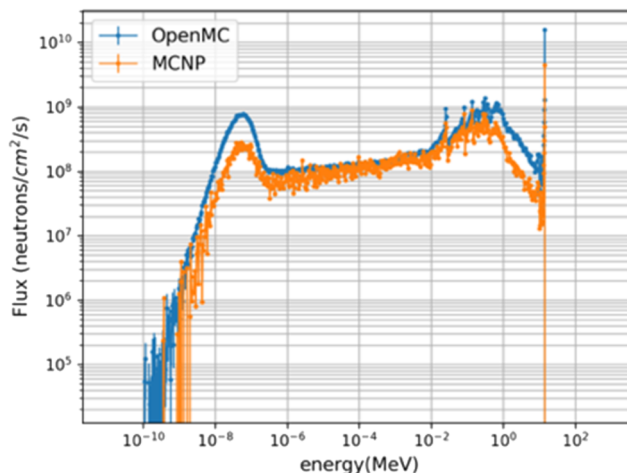

FIG. 2. OpenMC vs MCNP in a shell outside of the tokamak. Source rate = 5 $\times 10^{19}$ n/s.

run in 20° mode centered at 0° with reflective side boundaries as shown by the shaded area in Fig. 1(a).

Results are shown in Fig. 2. The OpenMC model generally agrees well with the CAD-based MCNP model, which proves the OpenMC model's reliability as a scoping tool. In the fast range, the OpenMC results are higher than the MCNP results by a factor of three because the 0-degree port shielding in MCNP is not as open as the one in OpenMC. The discrepancies in the thermal range might be due to the differences between the CSG-based and detailed CAD-based approaches. Thermal neutrons are less penetrating, so they are more likely to be affected by details in the geometry. However, thermal neutrons are of little interest in the neutron diagnostic system.
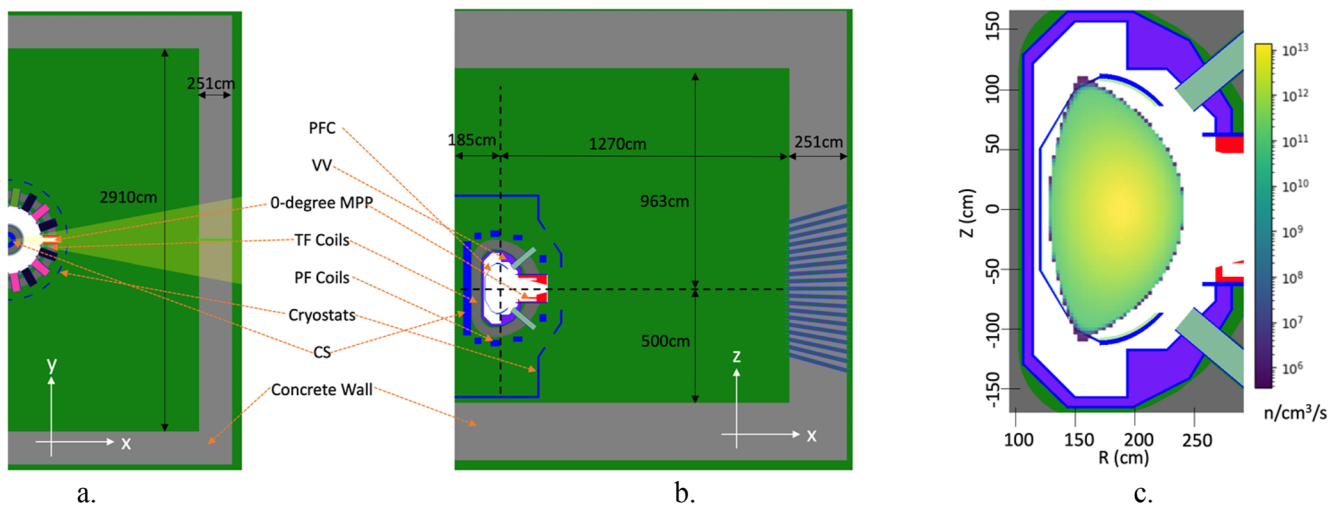
FIG. 1. OpenMC SPARC model. (a) XY view (+X half). (b) XZ view (+X half). (c) Neutron emissivity from TRANSP kinetic profiles. Dark gray: TF coils. Purple: VV. Red: 0MPP. Blue: Stainless steel parts, including CS, PF coils, and the cryostat. Dark green: Air. Light gray: concrete tokamak hall wall. On the +X wall are 19 collimators. See Sec. II A for the full names of the acronyms.

The 20° model is only used for verification. All other simulations in this paper were performed in 90° mode.

III. NEUTRON FLUX MONITORS

A. Neutrons in SPARC

A CAD-based MCNP-simulated fast neutron flux map is shown in Fig. 3. The source rate is 5×10^{19} n/s, corresponding to SPARC's 140 MW PRD. Compared to thermal neutrons undergoing extensive scatterings in the hall, fast neutrons retain more information about the plasma, so NFMs will be placed in the bright red/orange region to measure as many fast neutrons as possible while maintaining ease of construction. First, this does not put the NFMs in the way of other large components moving around in the tokamak hall; for example, when the port plugs need to be removed, we do not need to move the NFMs. In addition, because they will be installed on the wall instead of having a stand in the tokamak hall, they will not block the vision of other diagnostic systems. Finally, the length of the cables can be reduced from tens of meters to 5–10 m.

The layout of the NFM fleet is shown in Fig. 4. There are four B10 ICs, four U238 FCs, and more housing reserved for other NFMs. The central line of gray square tubes are collimators for neutron cameras[8] and a neutron spectrometer.[9] The rest of this section will discuss the neutronics aspect of the design of the flux-shaping materials for these NFMs.

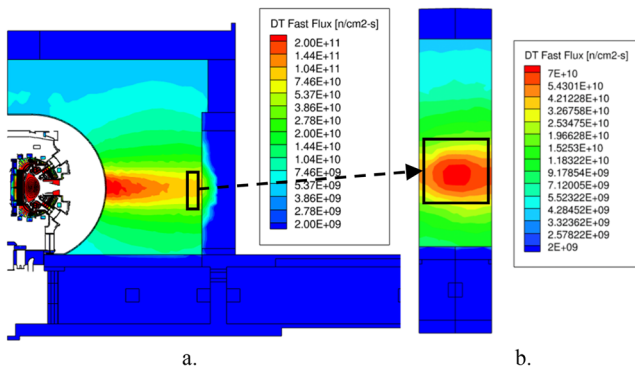Besides DT neutrons, 2.5 MeV DD neutrons are also a consideration for NFM designs: SPARC will have a dedicated DD campaign, and DD fusions are possible in DT plasma. As a result, B10 ICs shall have flat responses to DT and DD neutrons.

B. B10 coated gamma-compensated ionization chamber

B10 ICs detect neutrons by measuring B10 neutron absorption reaction products, which means detector responses should be proportional to the absorption rates. B10 ICs have high sensitivities thanks to B10's high thermal neutron absorption cross sections.[10] There are many off-the-shelf options, some with gamma compensation capabilities. Gamma noises, including neutron-induced gamma, fusion gamma, etc., are common in tokamak, so such capability to cancel gamma signals in the detector is highly desirable.

The proposed design of B10 IC is shown in Fig. 5. Since the B10 ICs are intrinsically sensitive to thermal neutrons while DT fusion neutrons are 14.1 MeV, a High-Density Polyethylene (HDPE) cylindrical sleeve is added to locally moderate fast neutrons. In addition, to filter out scattered neutrons from the surroundings so as to prioritize direct neutrons from the plasma, a Borated-HDPE (B-HDPE) housing with an opening facing toward the 0MPP is added. The housings are also expected to make calibration robust against changes in the tokamak hall, which can affect scattered neutrons and, therefore, potentially NFM responses. The performance
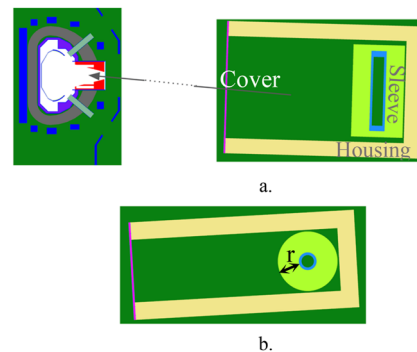
FIG. 5. (a) B10 IC side view (XZ). (b) B10 IC top/down view (XY). B10 IC and its shielding. Yellow: B-HDPE housing, Pink: B–Al cover. Light green: HDPE sleeve. Light blue: Aluminum case of the IC unit. The arrow indicates the direction the housing is facing.

FIG. 3. (a) XZ view. (b) YZ view by the wall. Fast (>1 MeV) neutron flux map in SPARC tokamak hall. Uncertainties in the tokamak hall <15%. Source rate = 5×10^{19} n/s.
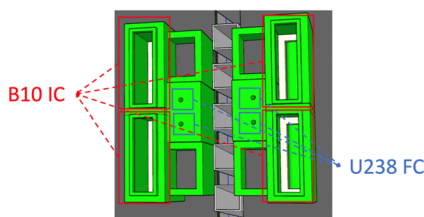
FIG. 4. NFM fleet layout. Dark gray: Concrete wall. Light gray: Collimators. Green: HDPE or B-HDPE.

FIG. 6. Neutron flux around the ICs with vs without the housing. Housing thickness = 5 cm. IC sleeve thickness = 6 cm. No B–Al cover. Source rate = 5×10^{19} n/s.

is under scoping. Finally, to cut off thermal neutrons from the front, a thin borated aluminum (B–Al) cover is added.

1. Housing

The housing wall thickness will be 5–10 cm. The final decision shall balance neutron shielding performance and volumes. Figure 6 compares neutron spectra around the IC units with and without the housing. The housing cuts ~80% <0.1 eV neutrons, ~50% <0.1 MeV neutrons, and has little effect on the 14 MeV peak, which fulfills its goals well.

2. Borated aluminum cover

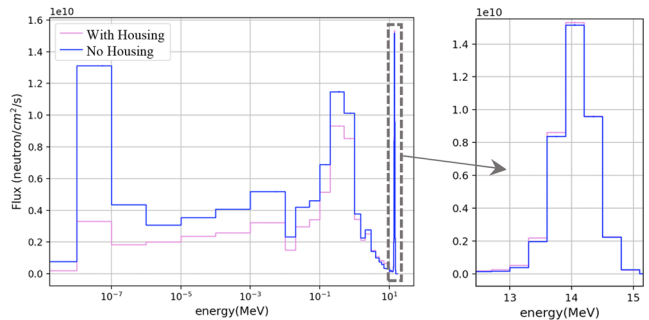The cover has a sandwich structure with 0.5 mm aluminum (Al) on both sides and 5 mm borated Al in the middle. To examine the effects of the cover, we tallied the neutron spectra inside the housings but outside of the sleeves. Results with 20% B4C + 80% Al cover, 40% B4C + 60% Al cover, and no cover are plotted in Fig. 7, and the relative differences are in Fig. 8. The cover reduces <1 eV neutrons by 20%–40% but cannot remove all of them since some are produced within the housing. The cover also slightly reduces higher-energy neutrons. In the 11–13 MeV range, cases with B–Al covers have slightly higher neutron flux. This could be due to the fact that 14 MeV neutrons are scattered into the 11–13 MeV range by the Al. The close performance of the 20% B4C and 40% B4C covers

indicates that 20% already cuts most of the thermal neutrons from the front and is enough for its purposes.

3. HDPE sleeves

Reasonably thick HDPE sleeves can better moderate fast neutrons and, therefore, improve the B10 IC's signals, but overly thick sleeves can block neutrons and reduce the signals. To quantify this effect, simulations were launched to compute the detector response as a function of sleeve thickness [r in Fig. 5(b)]. The 40% B–Al cover is used for this scoping. The results are summarized in Fig. 9. Note that (1) only the side thickness of the sleeve is varying while the top/bottom thickness stays at 2 cm, and (2) the inner width of the housing is changing to fit the sleeves while minimizing the width to better filter out thermal neutrons. The larger the housing openings are, the wider the fields of view (FOV) are, and the NFMs are seeing more regions other than the opening port. These regions are sources of scattered neutrons. Therefore, the housing openings should be as small as possible. As predicted, the detector response increases with increasing sleeve thickness for small sleeve thicknesses because of better moderation but then decreases due to blocking effects. 7 cm is the best for signal strength, while 12 cm provides a flat response.

FIG. 9. IC absorption rate vs sleeve thickness. Source rate = 5 × 10^{19} n/s.
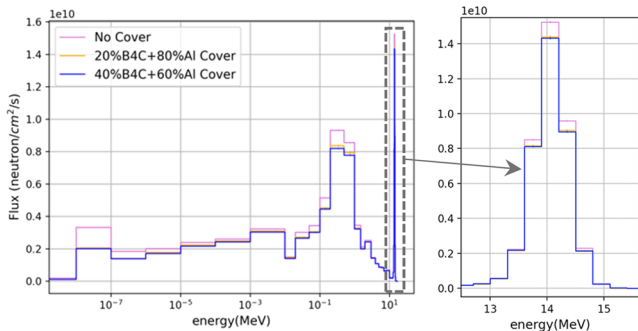
FIG. 7. Neutron flux inside the B10 IC housings. Sleeve thickness = 6 cm. Source rate = 5 × 10^{19} n/s.
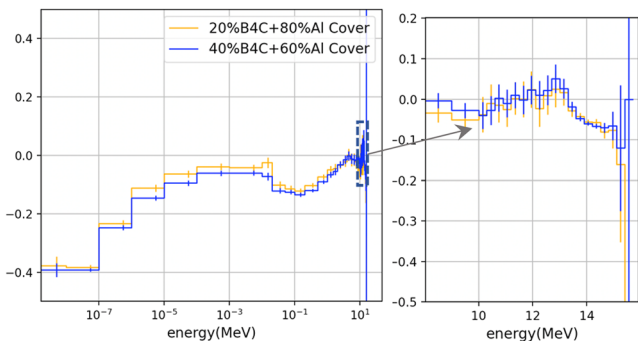
FIG. 8. Relative differences of Fig. 7 (with cover/no cover)-1.

FIG. 10. Neutron spectra inside the ICs and housings. Pink, orange, and blue are 2, 7, and 12 cm sleeve thicknesses, respectively. Thick lines refer to flux outside the sleeves while inside the housings. Thin lines refer to flux in the ICs' active volumes (the innermost green cylinder in Fig. 5(b)). Source rate = 5 × 10^{19} n/s.

TABLE I. Fast and thermal flux in housings and detectors ($n/cm^2/s$).

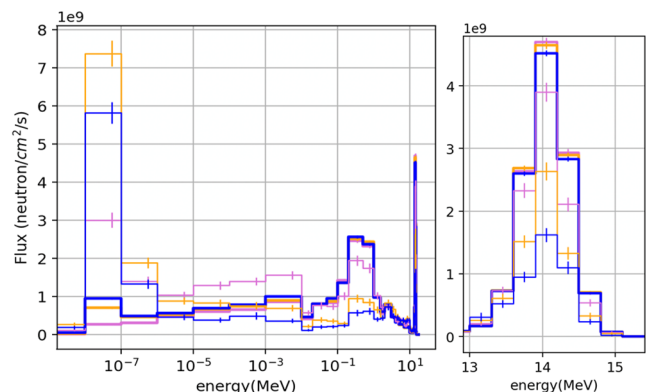| Sleeve	Energy	In housing	In detector
2 cm	Total	$8.90 \times 10^{10} \pm 5 \times 10^8$	$9.78 \times 10^{10} \pm 1.5 \times 10^9$
	<1 eV	$1.82 \times 10^9 \pm 5 \times 10^7$	$1.36 \times 10^{10} \pm 7 \times 10^8$
	>1 MeV	$5.40 \times 10^{10} \pm 4 \times 10^8$	$4.79 \times 10^{10} \pm 9.8 \times 10^8$
7 cm	Total	$2.94 \times 10^{10} \pm 1 \times 10^8$	$2.87 \times 10^{10} \pm 6 \times 10^8$
	<1 eV	$1.21 \times 10^9 \pm 2 \times 10^7$	$9.54 \times 10^9 \pm 4 \times 10^8$
	>1 MeV	$1.69 \times 10^{10} \pm 1 \times 10^8$	$1.29 \times 10^{10} \pm 3 \times 10^8$
12 cm	Total	$2.96 \times 10^{10} \pm 1 \times 10^8$	$2.14 \times 10^{10} \pm 5 \times 10^8$
	<1 eV	$1.49 \times 10^9 \pm 2 \times 10^7$	$7.35 \times 10^9 \pm 3.1 \times 10^8$
	>1 MeV	$1.65 \times 10^{10} \pm 9 \times 10^7$	$1.04 \times 10^{10} \pm 3 \times 10^8$

The 7 cm sleeve's detector response to DD plasma is slightly over-saturated, but, in reality, DD sources will be much lower than 5×10^{19} n/s.[3] The figure is meant to compare the relative sensitivity. DT and DD also have close responses with <2 cm sleeves. This could be because 2 cm is too thin as a moderator, and scattered neutrons dominate the detector's response, which is not what we want.

Neutron flux spectra of selected sleeve thicknesses are in Fig. 10. Neutron spectra outside the sleeves while inside the housings, representing pre-moderated fluxes, and those inside the detectors' active volumes, representing moderated fluxes, are compared.

As expected, there are more thermal neutrons and fewer fast neutrons after moderation. For the 2 cm sleeve, the 14 MeV peak only drops by about 20%, which confirmed that the 2 cm sleeve does not moderate direct neutrons well. The 12 cm sleeve moderates neutrons the best as it has the lowest 14 MeV peak inside, but the thermal flux inside is lower than the 7 cm sleeve because of block effects.

Quantitatively, according to Table I, there are only a few percent of <1 eV neutrons before moderation, and this ratio increases to >33% after moderation by the 7 and 12 cm sleeves, but only 14% by the 2 cm sleeve. As a result, the final decision will be between 6 and 14 cm depending on the *in situ* signal strength and engineering limitations such as volumes and weights.

4. Branching ratio

The use of current-mode B10 detectors assumes the 6:94 branching ratio[11] of $^{10}B(n,\alpha_0)$ and $^{10}B(n,\alpha_1)$, whose energy of product ions is 2.79 and 2.31 MeV, respectively. However, according to Fig. 8 in Ref. 11, this ratio is only valid for incident neutrons <100–200 keV. For the current mode of ICs, signal strength is related to the product ions' energies. This might be an issue for B10 ICs' performance in a fast neutron environment.

To evaluate this concern, energy-wise absorption rates of the B10 ICs with 7 and 12 cm HDPE sleeves are tallied and plotted in Fig. 11. The results confirmed that, in the SPARC environment, more than 99% of the absorptions are induced by neutrons <100 keV, which suggests that the energy dependence of the branching ratio will not affect the performance of B10 NFMs.

C. U238 fission chamber

The proposed U238 FC is a multilayer parallel plate FC operated in counter mode similar to the ones planned for use in ITER's
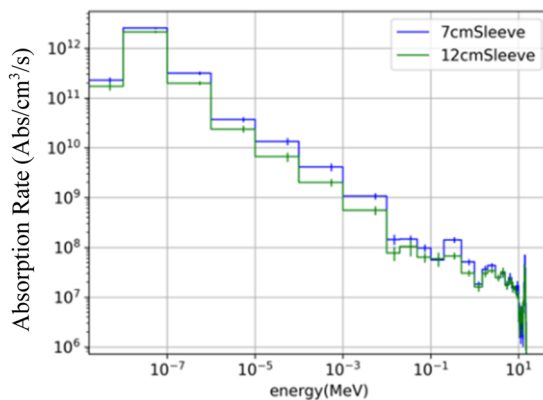

FIG. 11. B10 IC energy-wise neutron absorption rate. Source rate = 5×10^{19} n/s.

radial neutron camera.[12] Compared to B10, U238 is insensitive to thermal neutrons and, therefore, intrinsically prioritizes direct neutrons. A B-HDPE sleeve is added to prioritize fast neutrons further, as shown in Fig. 12. The 30-cm long front opening channel facing toward the 0° port provides a collimated FOV to the plasma.

OpenMC simulations of U238 FC are verified with the ToFu[13] code. ToFu calculates flux at a given location contributed by sources that can be seen "optically" at the location. ToFu results are analogous to uncollided neutron flux, despite some underestimation because ToFu does not count the neutrons penetrating through objects. Uncollided neutron flux at the end of the 30-cm long opening channel is computed by OpenMC and ToFu and compared. Their results agree well, as shown in Table II. OpenMC underestimates the flux instead of overestimating, mainly because OpenMC takes the attenuation in the air into account. The attenuation of 14.1 MeV neutrons in the air could be ~10% through 10 m.

OpenMC simulation results are shown in Table III. Thanks to the intrinsic form factor of U238 FCs and the sleeve, about 60% of the signals, i.e., fission reactions, are induced by direct neutrons. The FOV by the opening channel already covers the entire opening port. The direct/total ratio could be further improved by using a longer channel, which leads to a smaller FOV. Moreover, the 20 cm-thick sleeve and the 10 cm-thick one produce similar results within statistical errors, which means 10 cm is thick enough to shield out scattered neutrons from the side.
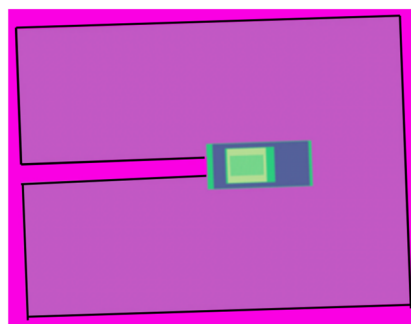

FIG. 12. U238 FC diagram. The black outline is the sleeve.

TABLE II. Neutron flux in U238 FC sleeve channel. Source rate = 5×10^{19} n/s.

OpenMC (uncollided)	$3.25 \times 10^{10} \pm 1.17 \times 10^9$
ToFu (optical)	3.57×10^{10}

TABLE III. Fission rate in U238 FC. Source rate = 5×10^{19} n/s.

Sleeve thickness (cm)	10	20
Total fission rate ($\#/cm^3/s$)	$6.10 \times 10^8 \pm 2.26 \times 10^7$	$5.96 \times 10^8 \pm 2.21 \times 10^7$
Direct fission rate ($\#/cm^3/s$)	$3.54 \times 10^8 \pm 1.77 \times 10^7$	$3.64 \times 10^8 \pm 1.82 \times 10^7$
Direct/total ratio	$58\% \pm 3.6\%$	$61\% \pm 3.8\%$

IV. CONCLUSIONS AND FUTURE WORK

In this work, we explored B10 gamma-compensated ICs and parallel-plate U238 FCs as NFMs for SPARC operation ranges. They are all proposed to be installed by the tokamak hall wall facing the opening $0°$ port on SPARC. A CSG-based OpenMC model has been used for the analysis.

The B10 ICs will have HDPE sleeves, B-HDPE housings, and B–Al covers. B-HDPE and B–Al combined effectively reduce scattered thermal neutrons and make >50% of neutrons around the ICs fast neutrons (>1 MeV). The HDPE sleeves create more thermal neutrons locally to improve detector responses. 7 cm thickness creates the strongest signal, and 12 cm gives flat responses to DT and DD plasma. In addition, >99% of the absorption reactions are induced by neutrons <100 keV in SPARC, which eliminates the concern of B10 absorption branching ratio.

The multilayer parallel plate U238 FCs, intrinsically insensitive to thermal neutrons, are equipped with thick B-HDPE sleeves with a 30-cm long opening channel facing the opening port to prioritize direct neutrons. As a result, 60% of the detector responses are induced by direct neutrons.

Next, we will test a U238 FC prototype in the laboratory, including angular dependence, pulse shape discrimination capability, sleeve performance, etc. In addition, more NFMs will be explored, including a Li-based scintillator and calibration range NFMs such as B10 proportional counters.

ACKNOWLEDGMENTS

AUTHOR DECLARATIONS

Conflict of Interest

All authors are financially supported by CFS either as employees or through sponsored research contracts. CFS is seeking to commercialize fusion energy and may benefit financially from the subject discussed in this paper.

Author Contributions

X. Wang: Conceptualization (equal); Data curation (equal); Formal analysis (equal); Investigation (equal); Methodology (equal); Software (lead); Visualization (lead); Writing – original draft (lead). **R. Gocht**: Conceptualization (equal); Formal analysis (equal); Investigation (equal); Methodology (equal); Validation (equal); Visualization (equal); Writing – review & editing (equal). **J. Ball**: Conceptualization (equal); Software (equal); Writing – review & editing (equal). **S. Mackie**: Conceptualization (equal); Software (equal); Writing – review & editing (equal). **E. Panontin**: Software (equal); Writing – review & editing (equal). **R.A. Tinguely**: Conceptualization (equal); Investigation (equal); Project administration (equal); Resources (equal); Supervision (lead); Writing – review & editing (equal). **P. Raj**: Investigation (equal); Project administration (equal); Supervision (equal); Writing – review & editing (equal). **I. Holmes**: Data curation (equal); Investigation (equal); Software (equal). **A.A. Saltos**: Data curation (equal); Methodology (equal); Software (equal). **A. Johnson**: Data curation (equal); Investigation (equal); Software (equal). **A. Grieve**: Data curation (equal); Investigation (equal); Software (equal).

DATA AVAILABILITY

The data that support the findings of this study are available from the corresponding author upon reasonable request.

REFERENCES

[1] P. Romano, N. Horelik, B. Herman, A. Nelson, B. Forget, and K. Smith, "OpenMC: A state-of-the-art Monte Carlo code for research and development," Ann. Nucl. Energy **82**, 90–97 (2015).

[2] A. J. Creely *et al.*, "Overview of the SPARC tokamak," J. Plasma Phys. **86**(5), 865860502 (2020).

[3] P. Raj *et al.*, "Overview of the preliminary design of SPARC's neutron diagnostic systems," in 25th Topical Conference on High Temperature Plasma Diagnostics, Asheville, NC, 2024.

[4] J. Breslau *et al.*, *TRANSP*, Computer software, USDOE Office of Science (SC), Fusion Energy Sciences (FES), 27 June 2018.

[5] P. Rodriguez-Fernandez *et al.*, "Predictions of core plasma performance for the SPARC tokamak," J. Plasma Phys. **86**(5), 865860503 (2020).

[6] H.-S. Bosch and G. Hale, "Improved formulas for fusion cross-sections and thermal reactivities," Nucl. Fusion **32**(4), 611 (1992).

[7] C. J. Werner *et al.*, MCNP6.2 Release Notes, report LA-UR-18-20808, Los Alamos National Laboratory, 2018.

[8] J. Ball *et al.*, "Design of a spectrometric detector unit for the SPARC neutron camera," in 25th Topical Conference on High Temperature Plasma Diagnostics, Asheville, NC, 2024.

[9] S. Mackie *et al.*, "Ion optical design of NSPC, the magnetic proton recoil neutron spectrometer for burning plasma diagnosis of the SPARC tokamak," in 25th Topical Conference on High Temperature Plasma Diagnostics, Asheville, NC, 2024.

[10] D. A. Brown *et al.*, "ENDF/B-VIII," Nucl. Data Sheets **148**, 1 (2018).

[11] F.-J. Hambsch and H. Bax, "The standard branching ratio $^{10}B(n, \alpha_0)$ to $^{10}B(n, \alpha_1)$," J. Nucl. Sci. Technol. **39**(sup2), 1402–1405 (2002).

[12] B. Esposito *et al.*, "Progress of design and development for the ITER radial neutron camera," J. Fusion Energy **41**(2), 22 (2022).

[13] D. Vezinet, L. S. Mendoza, F. L. Bourdais, J. Morales, and A. Khandelwal, "ToFu project Github," [Online]. Available: https://tofuproject.github.io/tofu/index.html.